There are various types of solar active regions...

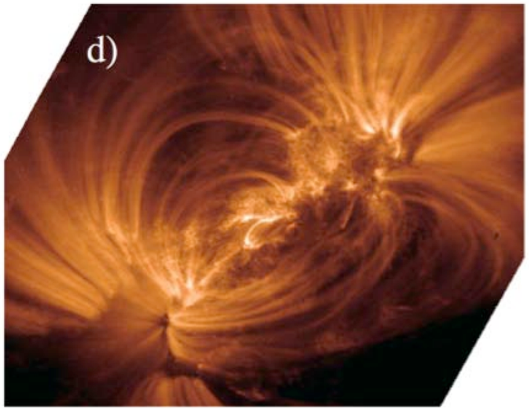

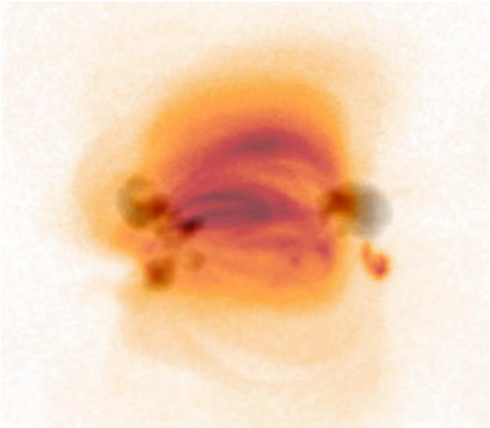

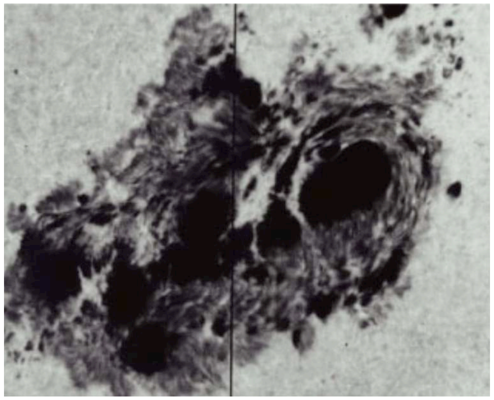

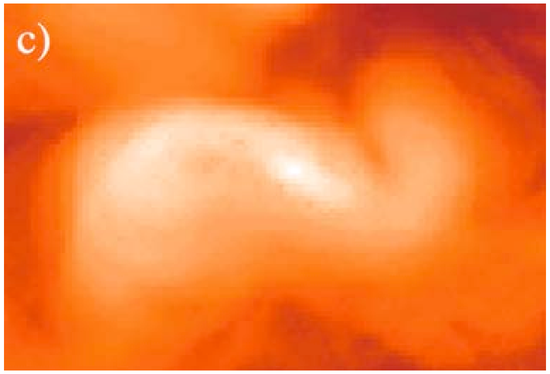

These active regions are developed from a common magnetic structure, i.e. twisted flux tube.

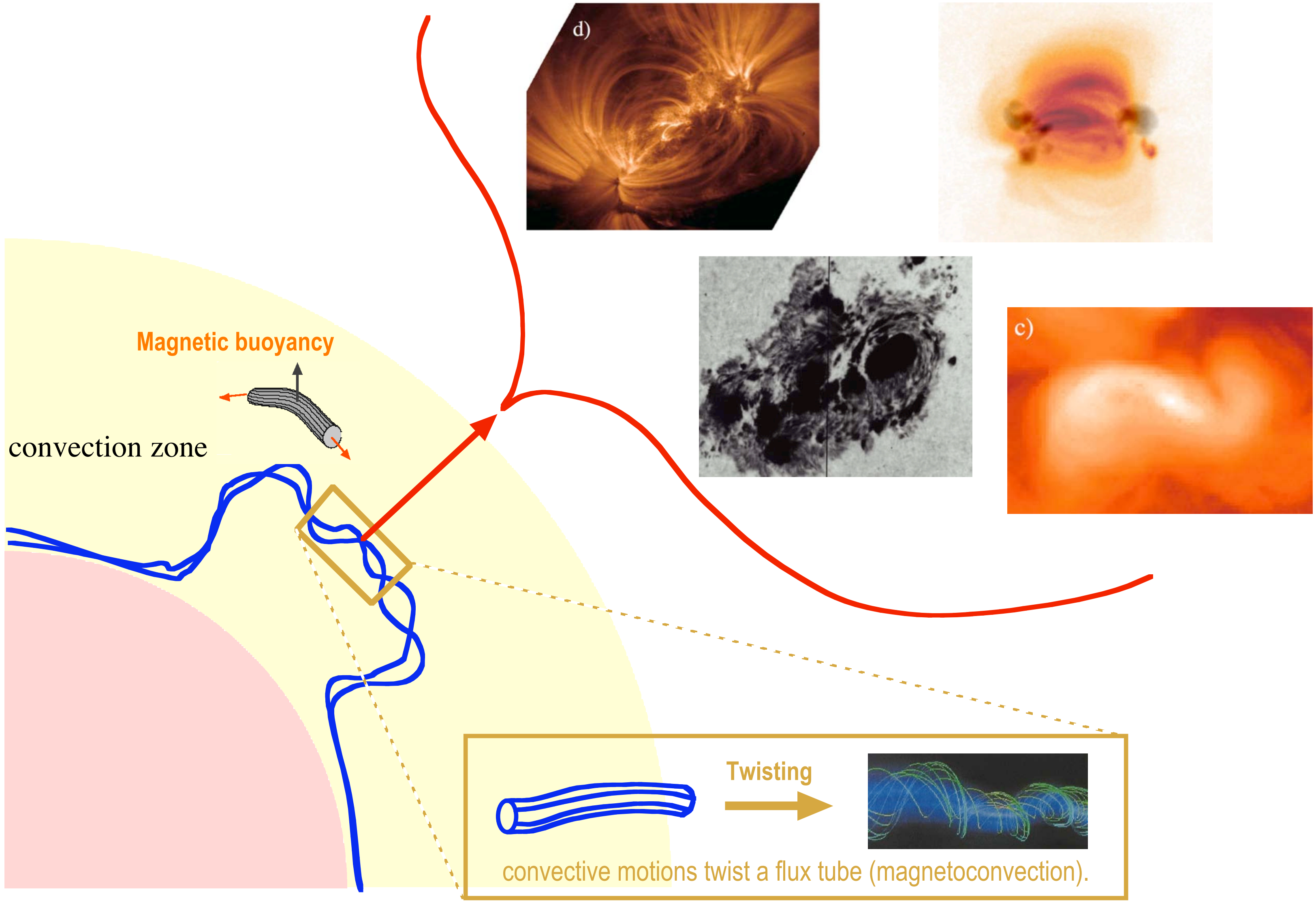

Similarity between solar active regions and animals...

Active regions

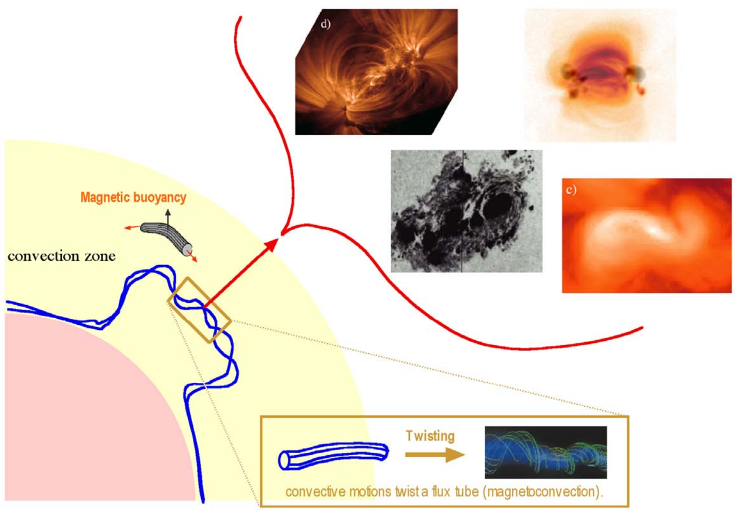

Animals

https://www.istockphoto.com/jp/%E3%83%99%E3%82%AF%E3%82%BF%E3%83%BC/%E7%94%9F%E7%89%A9%E3%81%AE%E9%8
0%B2%E5%8C%96%E3%81%AB%E3%82%B9%E3%82%AD%E3%83%BC%E3%83%A0%E3%81%AE%E9%80%B2%E5%8C%96-
animalschildren-%E3%81%AE%E6%95%99%E8%82%B2%E7%A7%91%E5%AD%A6%E3%81%BE%E3%81%99-gm486713328-735849

Their origins have simple structure.

Even though they have simple structure, these origins play fundamental roles in determining the characteristics of active regions/animals.

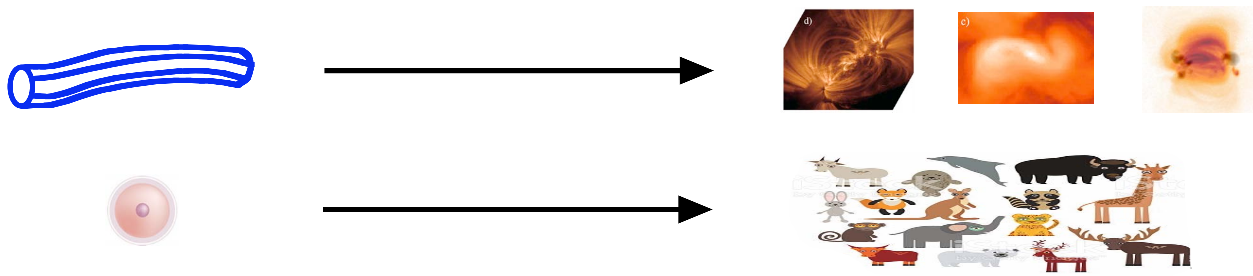

This suggests that physical properties of subsurface magnetic fields (twisted flux tube) characterize solar active regions.

However, it is difficult to obtain these properties <u>via direct observations using electromagnetic waves</u> (the surface of the Sun behaves like an impermeable boundary toward radiative flux).

Then what shall we do?

Forward problem vs. Inverse problem

Forward problem

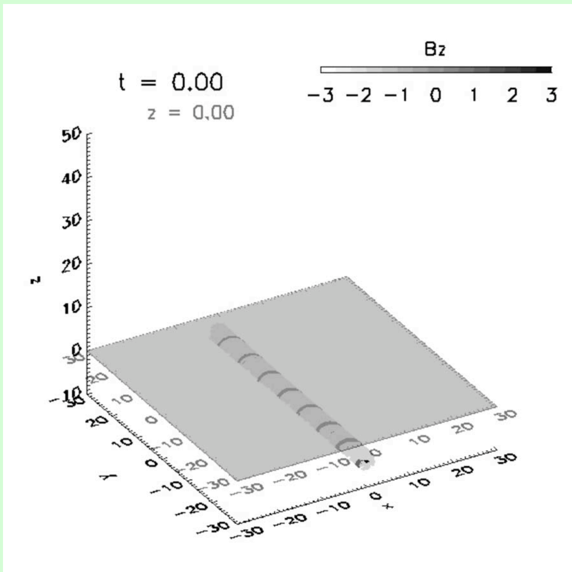

flux-emergence simulation

Physical properties of subsurface magnetic fields **(invisible cause)**... **input**

↓

Evolution of surface magnetic fields **(observed result)**... **derived**

Inverse problem

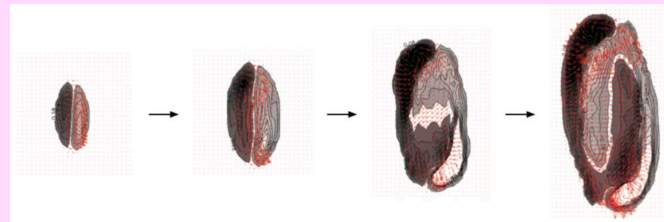

↓

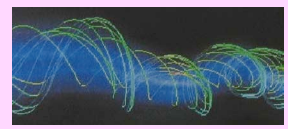

Evolution of surface magnetic fields **(observed result)**... **input**

↓

Physical properties of subsurface magnetic fields **(invisible cause)**... **derived**

By solving the inversion problem, we may derive physical properties of subsurface magnetic fields.

Surface magnetic fields have been classified on the basis of their morphological features.

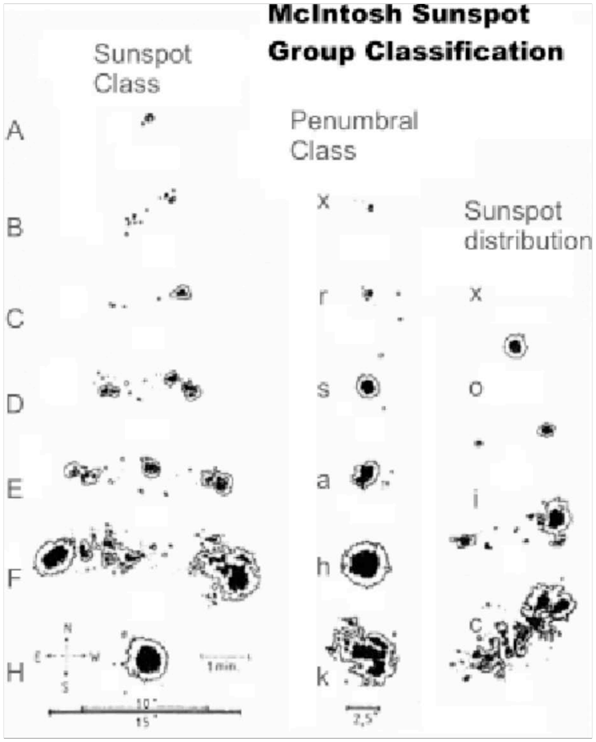

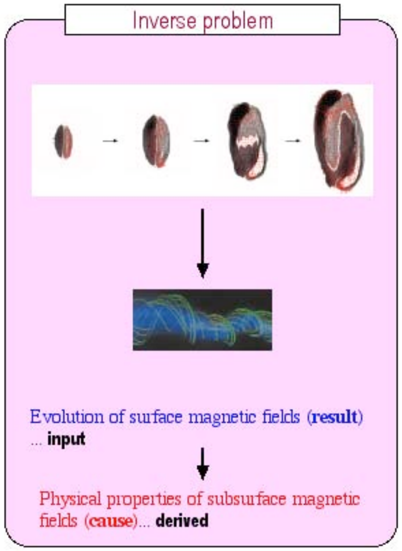

For solving the inverse problem, such morphological classification is insufficient to provide an input in the problem.

A quantitative representation of surface magnetic field evolution is necessary.

Quantitative representation of surface magnetic field evolution

Two key quantities obtained from observations of surface magnetic field evolution:

Emerged magnetic flux (Φ_{emg})... provides information on scales

Injected magnetic helicity (H_{inj})... provides information on configurations

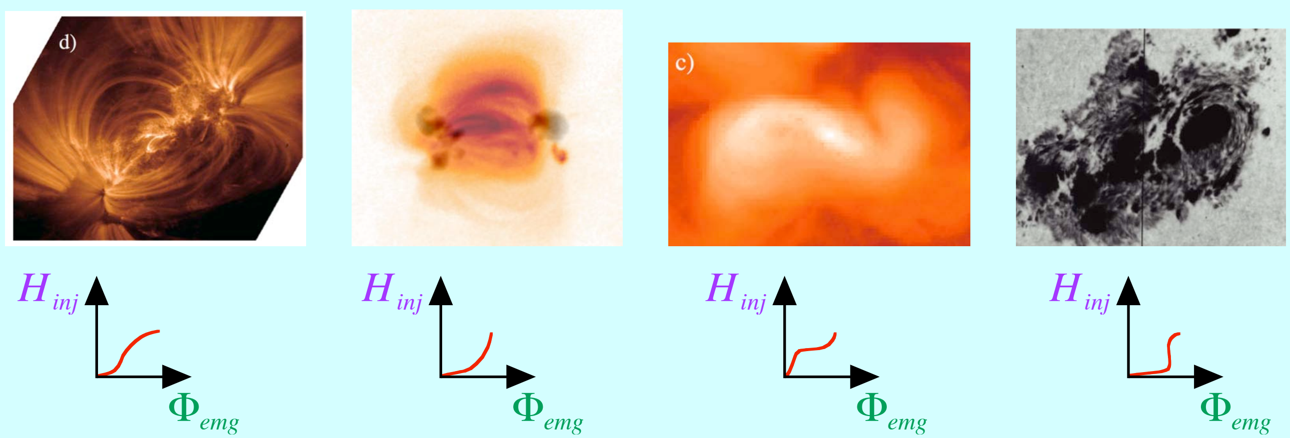

Each active region has its own profile in (Φ_{emg}, H_{inj})-space

=> evolutionary path of the active region

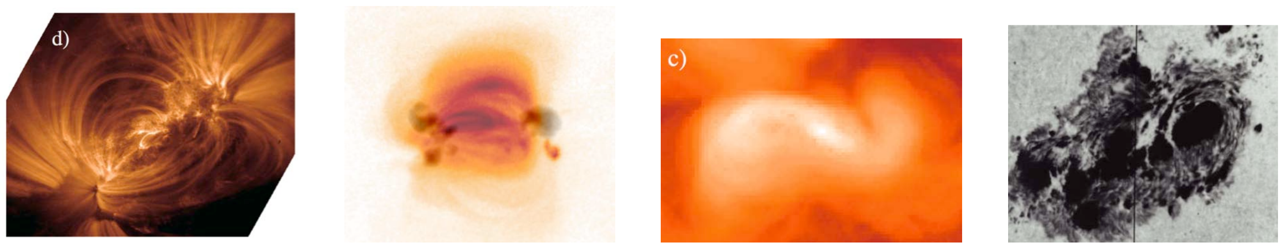

Morphological representation

Quantitative representation (evolutionary path)

Using the evolutionary path, we solve the inverse problem.

To derive physical properties of subsurface magnetic fields from the evolutionary path via inversion, we introduce a model of flux emergence.

R: radius of a flux tube h: height of emergence ($0 \le h \le 2R$)

L: length of emergence w: width of emergence ($w = \sqrt{(2R-h)h}$)

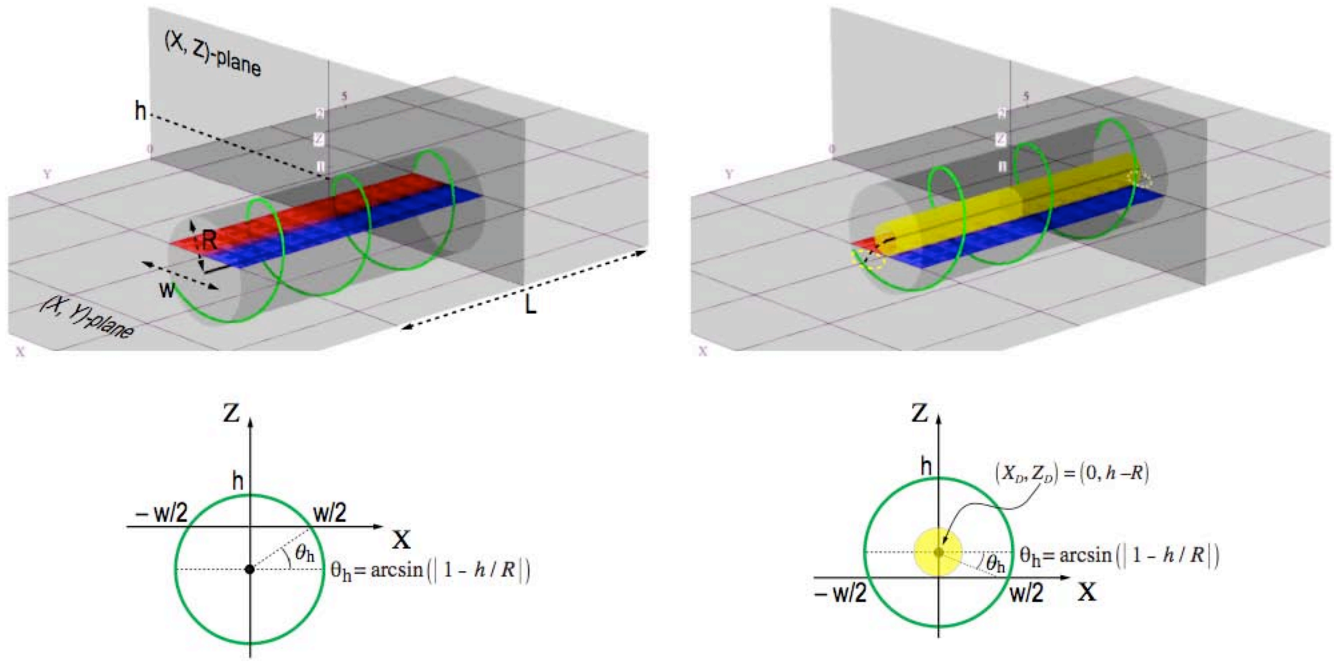

Phase I ($0 \le h \le R$)

Phase II ($R < h \le 2R$)

Left panel... axis of an emerging flux tube is below surface ($h \le R$)

Right panel... axis of an emerging flux tube is above surface ($h \ge R$)

The model provides key physical parameters that describe the properties and processes of subsurface magnetic fields...

Physical properties of subsurface magnetic fields: flux-tube radius, field strength, twist

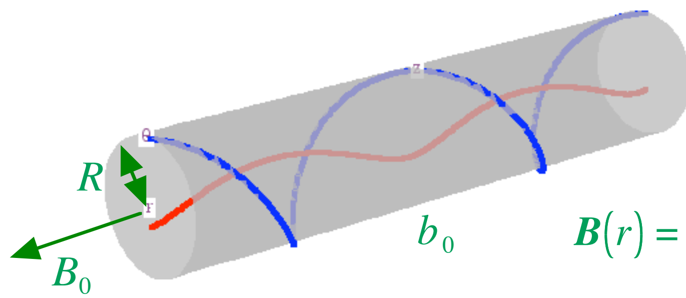

$$\boldsymbol{B}(r) = B_0 \frac{b_0\, r\, \hat{\theta} + \hat{a}}{1 + (b_0\, r)^2}$$

Time-dependent processes of flux emergence: emergence length, emergence height

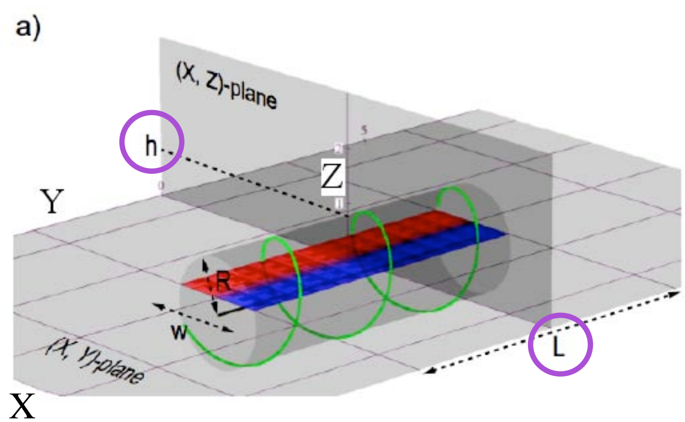

$$\begin{cases} h = h(t) \\ L = L(t) \end{cases} \longrightarrow h = \mathrm{fef}(L)$$

parametric equation (pair of time-dependent functions)

fef: **flux-emergence function**

Flux-emergence function... characterized by three parameters

$$h = \mathrm{fef}(L) \equiv \boxed{h_{max}} \sin\left[\frac{\pi}{2}\left(\frac{L}{\boxed{L_{max}}}\right)^{\boxed{\delta}}\right]$$

h_{max}: maximum emergence height

L_{max}: maximum emergence length

δ: parameter controlling how flux emergence proceeds

Examples of $h = \mathrm{fef}(L)$:

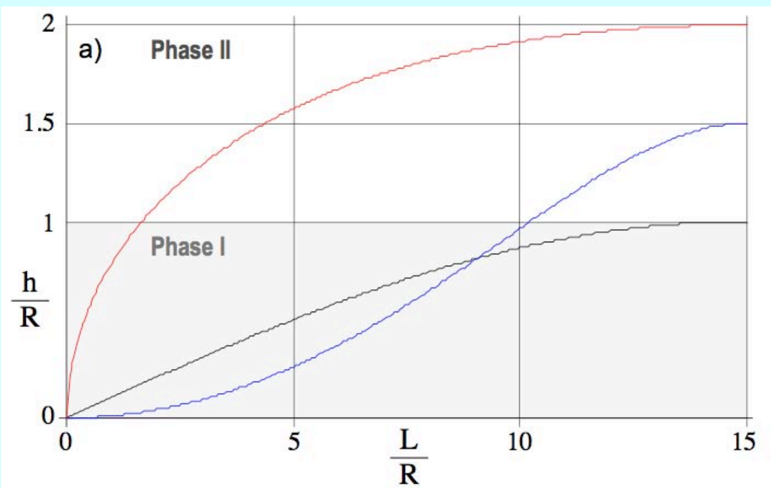

full-emergence $h_{max} = 2R,\ L_{max} = 15R,\ \delta = 0.5$

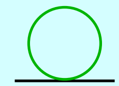

intermediate-emergence $h_{max} = 1.5R,\ L_{max} = 15R,\ \delta = 2$

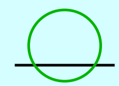

half-emergence $h_{max} = R,\ L_{max} = 15R,\ \delta = 1$

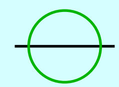

When δ takes a smaller value (red curve), flux-emergence proceeds actively at an early phase, then it becomes saturated, showing a relatively longer late phase.

Emerged magnetic flux & injected magnetic helicity calculated from the model...

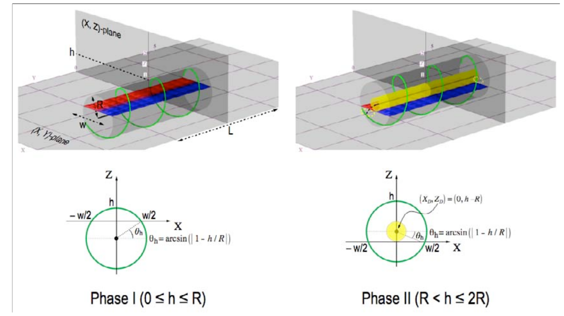

Emerged magnetic flux (Φ_{emg}):

- **Apparent emerged flux (Φ^{A}_{emg})**... signed flux crossing a horizontal plane (surface): directly observed

$$\Phi^{A}_{emg}(\text{Phase I}) = \frac{B_0 L}{|b_0|} \ln\left(\frac{1 + b_0^2 R^2}{1 + b_0^2 (R - h)^2}\right)$$

$$\Phi^{A}_{emg}(\text{Phase II}) = \frac{B_0 L}{|b_0|} \ln\left(\frac{1 + b_0^2 R^2}{\left[1 + b_0^2 (R - h)^2\right]^{1 - \frac{2\pi}{|b_0| L}}}\right)$$

- **Net emerged flux (Φ^{N}_{emg})**... unsigned flux crossing a vertical plane:

used for calculating injected magnetic helicity

Injected magnetic helicity (H_{inj}):

$$H_{inj}(\text{Phase I}) = \frac{B_0^2 L}{4 b_0^3}\left[(\pi - 2\theta_h)\left\{\ln\left(1 + b_0^2 R^2\right)\right\}^2 - \int_{\theta_h}^{\pi-\theta_h}\left\{\ln\left(1 + \frac{b_0^2 (R - h)^2}{\sin^2\theta}\right)\right\}^2 d\theta\right]$$

$$H_{inj}(\text{Phase II}) = \frac{B_0^2 L}{4 b_0^3}\left[(\pi + 2\theta_h)\left\{\ln\left(1 + b_0^2 R^2\right)\right\}^2 + \int_{\theta_h}^{\pi-\theta_h}\left\{\ln\left(1 + \frac{b_0^2 (R - h)^2}{\sin^2\theta}\right)\right\}^2 d\theta\right]$$

$$\theta_h = \arcsin\left(\left|1 - h / R\right|\right)$$

A set of six parameters in the model determine the evolutionary path of an active region...

Physical properties of subsurface magnetic fields: $R,\ B_0,\ b_0$

Time-dependent processes of flux emergence: $h_{\max},\ L_{\max},\ \delta$

$$\Phi^{A}_{emg}(\text{Phase I}) = \frac{B_0 L}{|b_0|} \ln\left(\frac{1 + b_0^2 R^2}{1 + b_0^2 (R-h)^2}\right)$$

$$\Phi^{A}_{emg}(\text{Phase II}) = \frac{B_0 L}{|b_0|} \ln\left(\frac{1 + b_0^2 R^2}{\left[1 + b_0^2 (R-h)^2\right]^{1-\frac{2\pi}{|b_0| L}}}\right)$$

$$H_{inj}(\text{Phase I}) = \frac{B_0^2 L}{4 b_0^3}\left[(\pi - 2\theta_h)\left\{\ln\left(1 + b_0^2 R^2\right)\right\}^2 - \int_{\theta_h}^{\pi-\theta_h}\left\{\ln\left(1 + \frac{b_0^2 (R-h)^2}{\sin^2\theta}\right)\right\}^2 d\theta\right]$$

$$H_{inj}(\text{Phase II}) = \frac{B_0^2 L}{4 b_0^3}\left[(\pi + 2\theta_h)\left\{\ln\left(1 + b_0^2 R^2\right)\right\}^2 + \int_{\theta_h}^{\pi-\theta_h}\left\{\ln\left(1 + \frac{b_0^2 (R-h)^2}{\sin^2\theta}\right)\right\}^2 d\theta\right]$$

$$\theta_h = \arcsin\left(\left|1 - h/R\right|\right)$$

Φ^{A}_{emg} and H_{inj} are expressed as functions of *h* and *L*.

$$\boxed{h = \mathrm{fef}(L)}$$

$$h = \mathrm{fef}(L) \equiv \boxed{h_{\max}} \sin\left[\frac{\pi}{2}\left(\frac{L}{\boxed{L_{\max}}}\right)^{\boxed{\delta}}\right]$$

$$\Phi^{A}_{emg} = \Phi^{A}_{emg}(L)$$
$$H_{inj} = H_{inj}(L)$$

parametric equation

$$H_{inj} = f\left(\Phi^{A}_{emg};\ R,\ B_0,\ b,\ h_{\max},\ L_{\max},\ \delta\right)$$

Examples of the evolutionary path...

Flux-emergence function: $h = \mathrm{fef}(L)$

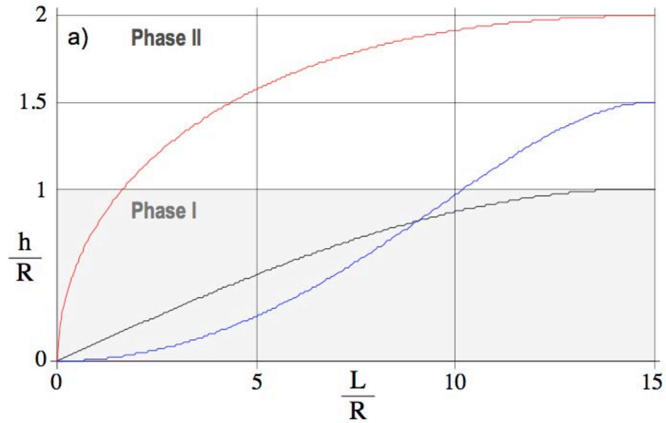

full-emergence $h_{max} = 2R,\ L_{max} = 15R,\ \delta = 0.5$

intermediate-emergence $h_{max} = 1.5R,\ L_{max} = 15R,\ \delta = 2$

half-emergence $h_{max} = R,\ L_{max} = 15R,\ \delta = 1$

Evolutionary path (solid line): $H_{inj} = f\left(\Phi_{emg}^{A}\right)$

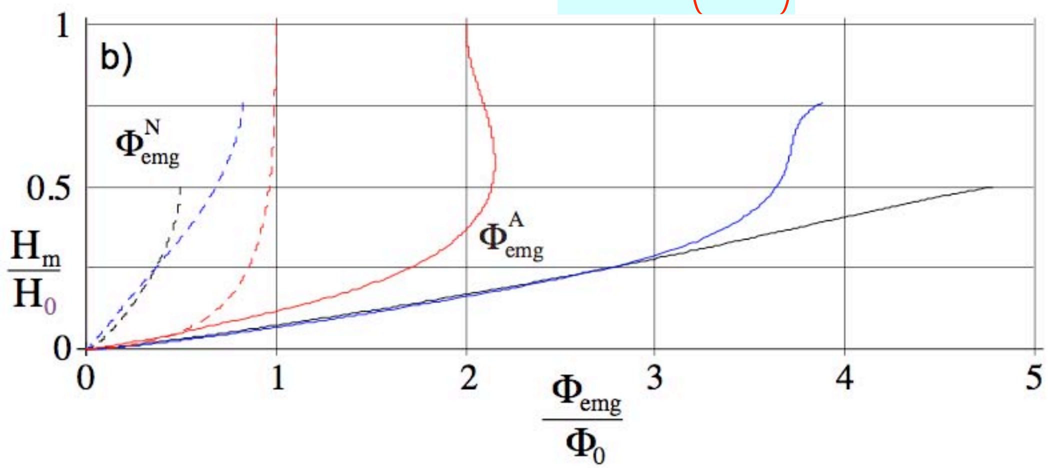

$$\Phi_0 = \frac{\pi B_0}{b_0^2} \ln\left(1 + b_0^2 R^2\right)$$
... total net flux

$$H_0 = \frac{b_0}{2\pi} \Phi_0^2 L_{max}$$
... maximum helicity

$b_0 = 1 / R$

Inversion (curve-fitting analysis)...

Model:

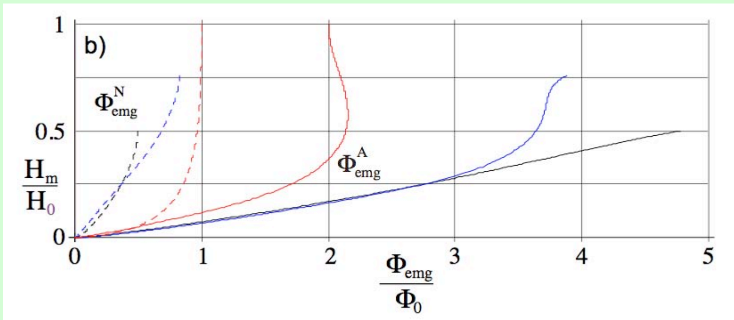

$$H_{inj} = f\left(\Phi^A_{emg}; R, B_0, b, h_{max}, L_{max}, \delta\right)$$

six parameters

Physical properties of subsurface magnetic fields: R, B_0, b_0

Time-dependent processes of flux emergence: h_{max}, L_{max}, δ

Evolutinary path obtained from surface magnetic field observation:

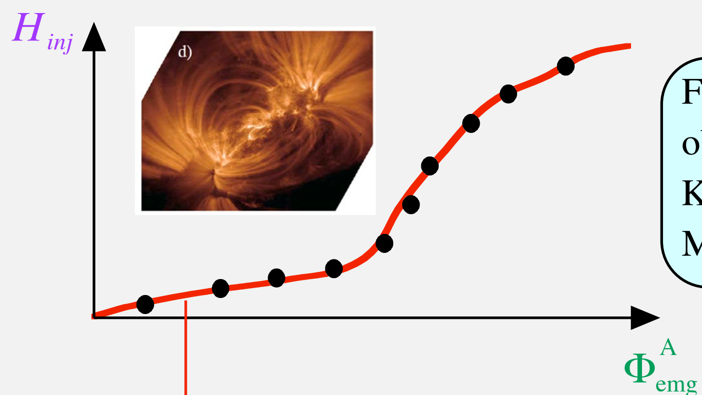

For estimating injected magnetic helicity from observed data, there are several methods (Chae 2001; Kusano et al. 2002; Démoulin & Berger 2003; Magara & Tsuneta 2008).

curve fitting => determine the six parameters

$$R, B_0, b_0 \;\; h_{max}, L_{max}, \delta$$

Check how well the inversion works (use simulated data)

(Magara 2017)

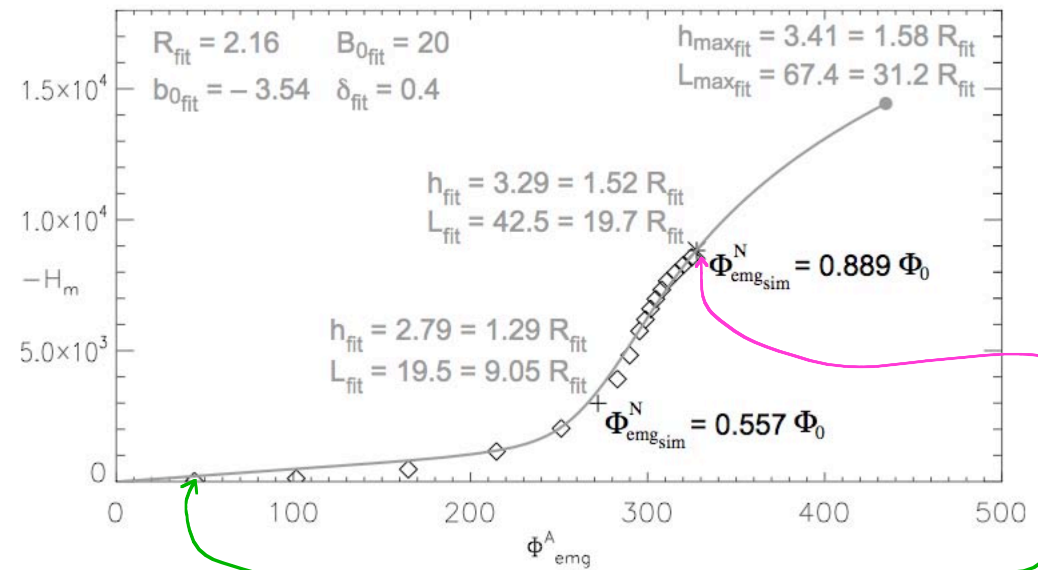

Figure 3. Data points (simulation) and a fitting curve (inversion) are presented in $(\Phi^A_{\mathrm{emg}}, H_{\mathrm{m}})$-space, which are drawn in black and gray, respectively. + and $*$ show a half-emergence state and the state shown by right panel of Fig. 1b.

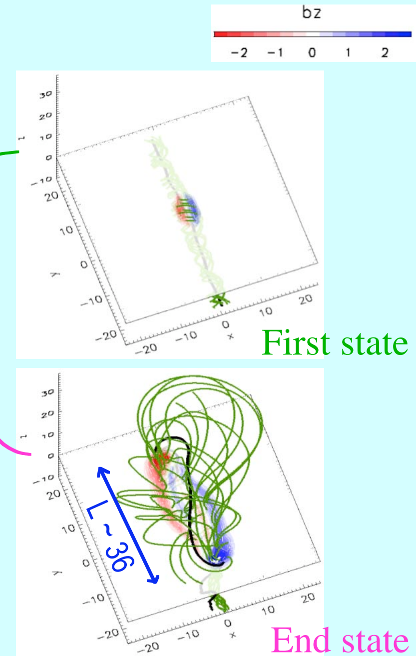

	simulation	inversion
R	2	2.16
B_0	17.4	20
b_0	– 1 (left-handed twist)	– 3.54
L	~ 36 (final state)	42.5

A possible explanation of this discrepancy is that after they emerge, magnetic field lines tend to be twisted strongly around their footpoints at the surface, which may enhance the inversion value compared to the uniform twist value assumed initially in the simulation.